Journal of Electronic Research and Application, 2026, Volume 10, Issue 7
http://ojs.bbwpublisher.com/index.php/JERA
Online ISSN: 2208-3510
Print ISSN: 2208-3502

Post-Grasp Pose Adjustment of a Tendon-Driven Underactuated Robotic Hand Using Finite-Action-Set Receding-Horizon Planning

Lei Hu, Hongran Li*

Jiangsu Ocean University, Lianyungang, Jiangsu, China

***Corresponding author**: Hongran Li, lihongran@jou.edu.cn

Abstract: This paper addresses local post-grasp pose adjustment for a tendon-driven underactuated robotic hand. A finite-action-set receding-horizon motor reference planning method is proposed, in which the continuous motor reference increment is discretized into representative actions and an action-effect table predicts local object pose changes. At each decision instant, candidate action sequences are evaluated using pose error, action magnitude, motor limits, grasp margin, and action switching, while only the first action of the optimal sequence is executed. Simulations show that the method generates feasible commands for single-axis and two-dimensional pose adjustment, drives the object pose toward the target, and keeps motor references within the allowable range. Compared with one-step planning, a longer prediction horizon reduces action switching in the two-dimensional coupled task and improves action sequence smoothness.

Keywords: Underactuated robotic hand; Tendon-driven; Post-grasp pose adjustment; Finite action set; Receding-horizon planning

Online publication: Aug 11, 2026

1. Introduction

Multi-fingered robotic hands can provide multiple contact points and flexible grasp postures, and therefore have important potential in robotic grasping and manipulation. Tendon-driven underactuated robotic hands have attracted increasing attention because of their compact structure, reduced number of actuators, lightweight design, and simple command interface [1–3]. However, a single motor usually affects multiple joints through tendon transmission, so the motor input, joint motion, and object pose response are strongly coupled. As a result, fine post-grasp pose adjustment is difficult to achieve through independent joint regulation.

In practical manipulation tasks, establishing a stable grasp is often not sufficient. After an object is grasped, small pose corrections may still be required, such as adjusting the tilt angle, changing the local orientation, or compensating for pose deviation caused by contact. Related problems have been studied through in-hand reorientation, multi-modal planning, trajectory optimization, model predictive control, feedback control, and action primitives [4–11]. Nevertheless, for tendon-driven underactuated hands, the object pose response is affected by contact location, friction condition, object shape, and finger configuration. Generating executable adjustment commands without relying on a complete contact dynamics model therefore remains challenging.

Model-driven methods can describe mechanical relationships during manipulation, but often require high modeling and computational effort and are sensitive to contact states and object parameters [6,13,14,18]. Learning-based methods can learn complex manipulation strategies from interaction data, but usually require many training samples, and their interpretability and transferability remain limited [9,12,15,16]. In comparison, finite-action-set methods reduce online decision complexity by converting continuous control inputs into a small number of representative actions [17]. However, simple one-step action selection may ignore the influence of the current action on subsequent adjustment steps, leading to frequent action switching or insufficiently smooth adjustment.

To address this problem, this paper proposes a finite-action-set receding-horizon motor reference planning method for post-grasp local pose adjustment of a tendon-driven underactuated robotic hand. The initial grasp is assumed to be stable, and the focus is upper-level generation of executable motor reference increment sequences rather than grasp control or contact force allocation. The continuous motor reference increment is discretized into a finite action set, and an action-effect table describes the average influence of each action on the local object pose. At each decision instant, the planner evaluates candidate action sequences over a finite horizon and considers pose error, action magnitude, motor limits, grasp margin, and action switching.

2. Materials and methods

2.1. System description and problem formulation

This study considers local post-grasp pose adjustment after a tendon-driven underactuated robotic hand has established a stable grasp. The object is held by the fingers, and the upper-level planner generates motor reference commands to move the object toward a desired local pose gradually. The planning variable is selected in the motor reference space because it is directly executable by the lower-level motor controller and avoids explicit optimization of joint torques, contact forces, or tendon tensions.

For the i-th finger, the tendon transmission relationship is written as

$$l_i = r_i\theta_i - A_i q_i - l_{0,i} \tag{1}$$

where the symbols denote the tendon length variation, motor spool radius, joint angle vector, geometric coupling matrix, and initial length offset, respectively. At each decision instant, the planner selects a motor reference increment and updates the reference command. The increment and the motor reference are both constrained to prevent abrupt motion and to keep the command within the allowable actuation range.

For the single-axis task, the object state is represented by the tilt angle. For the two-dimensional task, the state includes the tilt angle and the in-plane rotation angle. Given the desired pose, the post-grasp adjustment task is formulated as finite action sequence generation:

$$\min_{a_{0:K-1}} \sum_{k=0}^{K} \| s_d - s_k \|_Q^2 + \frac{\lambda_\theta \sum_{k=0}^{K-1} \| a_k}{\delta \|^2} + \lambda_l \sum_{k=0}^{K-1} P_{lim}\left(k\right) + \lambda_s \sum_{k=0}^{K-1} P_{stab}\left(k\right), a_k \in A \tag{2}$$

Here, A is the finite action set, δ is the basic action step, P_{lim} penalizes unsafe proximity to motor limits, and P_{stab} penalizes insufficient grasp margin. This formulation focuses on upper-level reference planning after grasp establishment, rather than complete grasp stability control.

2.2. Finite action set and pose prediction

The continuous motor reference increment is discretized into a small set of representative actions. Each action is represented by a normalized increment vector and scaled by the basic action step. In the simulation, the step size is 3°, and the motor order is thumb, index finger, middle finger, ring finger, and pinky finger. Only the thumb, index finger, and middle finger are assigned nonzero increments, while the ring finger and pinky finger provide auxiliary support. **Table 1** combines the finite action set and the nominal action effects. The two effect columns describe the average changes in tilt angle and in-plane rotation angle, respectively.

Table 1. Finite action set and nominal action effects

Action	sigma	Tilt effect	Rotation effect
a0	[0,0,0,0,0]	0.0	0.0
a1	[1,0,0,0,0]	0.4	-0.8
a2	[0,1,0,0,0]	0.9	0.5
a3	[0,0,1,0,0]	0.7	-0.3
a4	[-1,0,0,0,0]	-0.4	0.8
a5	[0,-1,0,0,0]	-0.9	-0.5
a6	[0,0,-1,0,0]	-0.7	0.3
a7	[1,-1,0,0,0]	1.0	-1.2
a8	[-1,1,0,0,0]	-1.0	1.2
a9	[0,1,-1,0,0]	1.3	0.8
a10	[0,-1,1,0,0]	-1.3	-0.8

At each decision step, actions that would violate the motor limits are excluded. The predicted pose is obtained by adding the nominal action effect to the current pose. To model the mismatch between the nominal table and the actual response, the simulated pose update is

$$s_{k+1} = s_k + \left(1 + \rho_k\right) \mu_{i_k} + \xi_k \tag{3}$$

where the selected action index determines the nominal action effect, the proportional action-effect error is sampled from a uniform distribution, and the last term represents zero-mean Gaussian measurement noise.

2.3. Receding-horizon planning and simulation settings

At each decision step, the planner observes the current object pose and motor reference, constructs the feasible action set, and evaluates candidate sequences over the prediction horizon. Starting from the current state, the predicted pose and motor reference are propagated using the action-effect table, and sequences that violate motor limits are discarded. Candidate sequences are evaluated by

$$J = \sum_{h=1}^{H} \lambda_e^h \| s_d - \hat{s}_{k+h} \|_Q^2 + \frac{\lambda_\theta \sum_{h=0}^{H-1} \| a_{i_h}}{\delta \|^2} + \lambda_l \sum P_{lim} + \lambda_s \sum P_{stab} + \lambda_c \sum P_{chg} \tag{4}$$

Only the first action of the optimal sequence is executed, and the same optimization is repeated after the object pose is updated. The loop stops when the pose error is below the prescribed threshold or the maximum number of decision steps is reached. The main simulation settings are as follows: motor reference range 0–90°, initial reference. $[45,45,45,45,45]^T$ deg, prediction horizon $H=3$, maximum step number 50, maximum action-effect error 0.1, measurement noise standard deviation 0.1°, and 20 repeated trials for each target. The stopping threshold is 1.0° for the single-axis task and 1.5° for the two-dimensional task. The weights are $\lambda_e = 1.0$, $\lambda_\theta = 0.05$, $\lambda_l = 50$, $\lambda_s = 10$, and λ_c=0.1. Reported metrics include final error, average error, adjustment steps, action energy, and successful trials

3. Simulation results

3.1. Single-axis pose adjustment

The first simulation evaluates single-axis pose adjustment. The object is initially placed at zero tilt, and the target tilt angle is selected from 10°, 15°, 20°, -10°, -15°, and -20°. **Figure 1** shows a representative result for the 20° target.

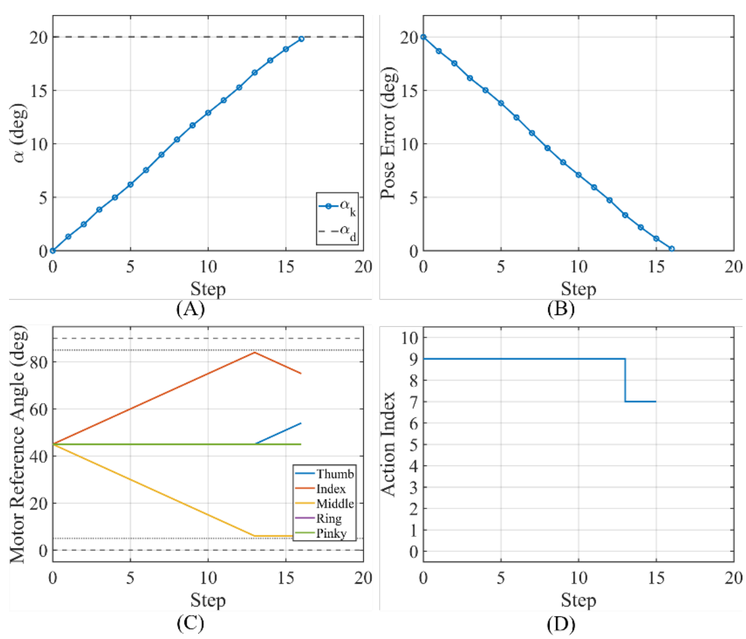

Figure 1. Single-axis pose adjustment result for the 20° target. (A) Object tilt angle. (B) Pose error. (C) Motor reference angles. (D) Selected action sequence.

As shown in **Figure 1**, the object tilt angle gradually approaches the target and the pose error decreases to the target neighborhood. The motor reference angles remain within the allowable range, indicating that the generated commands satisfy the actuation constraints. **Table 2** summarizes the results over all single-axis targets. All repeated trials reached the prescribed stopping threshold, and the mean final error remained below 0.64° for all targets.

Table 2. Single-axis pose adjustment results

Target (°)	Final error (°)	Average error (°)	Steps	Action energy
10	0.50	5.24	7.35	14.60
15	0.43	7.69	11.25	22.30
20	0.63	10.03	15.40	30.80
-10	0.48	5.23	7.45	14.80
-15	0.44	7.71	11.30	22.60
-20	0.57	9.97	15.45	30.90

3.2. Two-dimensional pose adjustment

The second simulation evaluates two-dimensional local pose adjustment, where the object pose includes the tilt angle and the in-plane rotation angle. The initial pose is $[0°, 0°]^T$. Figure 2 shows a representative result for the target. $[15°, -8°]^T$.

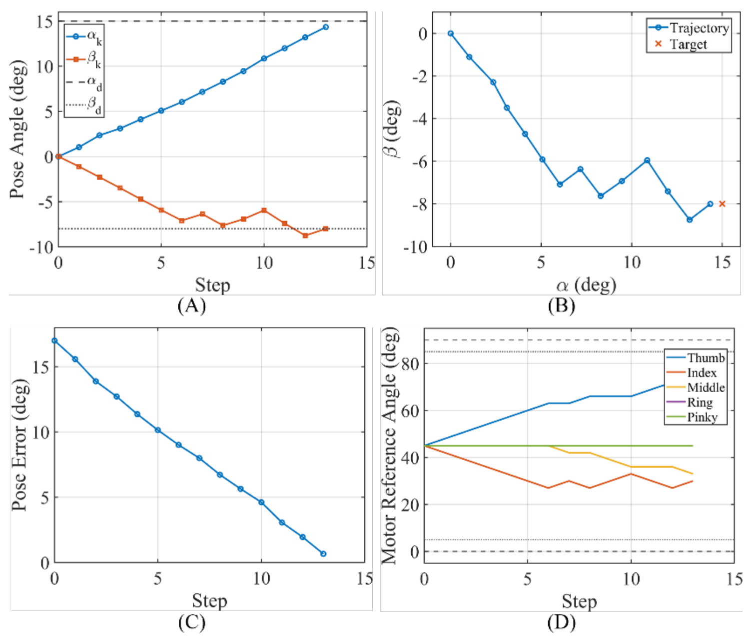

Figure 2. Two-dimensional pose adjustment result for the target $[15°, -8°]^T$. (A) Pose angles. (B) Pose trajectory in the alpha-beta plane. (C) Pose error norm. (D) Motor reference angles.

Figure 2 shows that the planner can regulate two coupled pose components using the same finite action set. Since each selected action may influence both pose components, the trajectory is not expected to be a straight line in the pose plane. Even so, the pose moves toward the target, the error norm decreases, and the motor references remain within the predefined limits. **Table 3** lists the statistical results for all two-dimensional targets. The mean final errors were all below 1.16°, and all repeated trials reached the stopping threshold.

Table 3. Two-dimensional pose adjustment results

Target pose (°)	Final error (°)	Average error (°)	Steps	Action energy
$[10,5]^T$	1.05	5.94	7.15	14.15
$[15,-8]^T$	0.99	8.68	12.95	25.80
$[-10,8]^T$	1.16	6.61	8.65	17.10
$[-15,-10]^T$	0.96	9.43	11.30	22.55
$[20,0]^T$	0.94	10.28	16.25	32.40

An additional comparison between $H=1$ and $H=3$ showed that both settings reached the prescribed stopping threshold in all tested trials. In the two-dimensional task, the average number of action switches decreased from 3.70 for *for* 3.13 fo$H=3$, while the accuracy-related metrics remained close. This suggests that the longer prediction horizon mainly improves action sequence smoothness rather than final pose accuracy under the present simulation settings. These numerical results support the feasibility of the proposed upper-level planner, but they do not imply guaranteed convergence under arbitrary contact conditions or direct validation on a physical robotic hand.

4. Conclusion

This paper investigated local post-grasp pose adjustment for a tendon-driven underactuated robotic hand and proposed a finite-action-set receding-horizon motor reference planning method. The continuous motor reference increment was discretized into representative actions, and a nominal action-effect table was used for local pose prediction. At each decision instant, the planner evaluated candidate sequences by considering pose error, action magnitude, motor limits, grasp margin, and action switching, executed only the first action of the optimal sequence, and replanned after feedback was obtained.

Simulation results showed that the proposed method can generate feasible motor reference increment sequences for both single-axis and two-dimensional local pose adjustment tasks. The object poses gradually approached the target neighborhood while the motor references remained within the allowable range. Compared with one-step planning, the $H=3$ setting reduced action switching in the two-dimensional task while maintaining comparable accuracy-related performance. Future work will focus on physical experiments, online updating of the action-effect table, and integration of tactile or contact feedback.

Disclosure statement

The authors declare no conflict of interest.

References

[1] Li H, Ford C, Bianchi M, et al., 2022, BRL/Pisa/IIT SoftHand: A Low-Cost, 3D-Printed, Underactuated, Tendon-Driven Hand with Soft and Adaptive Synergies. IEEE Robotics and Automation Letters, 7(4): 8745–8751.

[2] Zhou X, Fu H, Shentu B, et al., 2024, Design and Control of a Tendon-Driven Robotic Finger Based on Grasping Task Analysis. Biomimetics, 9(6): 370.

[3] Li G, Liang X, Gao Y, et al., 2024, A Linkage-Driven Underactuated Robotic Hand for Adaptive Grasping and In-Hand Manipulation. IEEE Transactions on Automation Science and Engineering, 21(3): 3039–3051.

[4] Morgan A, Hang K, Wen B, et al., 2022, Complex In-Hand Manipulation Via Compliance-Enabled Finger Gaiting and Multi-Modal Planning. IEEE Robotics and Automation Letters, 7(2): 4821–4828.

[5] Chen T, Tippur M, Wu S, et al., 2023, Visual Dexterity: In-Hand Reorientation of Novel and Complex Object Shapes. Science Robotics, 8(84): eadc9244.

[6] Jiang Y, Yu M, Zhu X, et al., 2024, Contact-Implicit Model Predictive Control for Dexterous In-Hand Manipulation: A Long-Horizon and Robust Approach. 2024 IEEE/RSJ International Conference on Intelligent Robots and Systems: 5260–5266.

[7] Yu M, Jiang Y, Chen C, et al., 2025, Robotic In-Hand Manipulation for Large-Range Precise Object Movement: The RGMC Champion Solution. IEEE Robotics and Automation Letters, 10(5): 4738–4745.

[8] Sieler A, Brock O, 2023, Dexterous Soft Hands Linearize Feedback-Control for In-Hand Manipulation. 2023 IEEE/RSJ International Conference on Intelligent Robots and Systems: 8757–8764.

[9] Saito D, Kanehira A, Sasabuchi K, et al., 2024, APriCoT: Action Primitives Based on Contact-State Transition for In-Hand Tool Manipulation. 2024 IEEE-RAS 23rd International Conference on Humanoid Robots: 827–834.

[10] Bircher W, Morgan A, Dollar A, 2021, Complex Manipulation with a Simple Robotic Hand Through Contact Breaking and Caging. Science Robotics, 6(54): eabd2666.

[11] Teeple C, Aktas B, Yuen M, et al., 2022, Controlling Palm-Object Interactions Via Friction for Enhanced In-Hand Manipulation. IEEE Robotics and Automation Letters, 7(2): 2258–2265.

[12] Yu C, Wang P, 2022, Dexterous Manipulation for Multi-Fingered Robotic Hands with Reinforcement Learning: A Review. Frontiers in Neurorobotics, 16: 861825.

[13] Chen T, Xu J, Agrawal P, 2021, A System for General In-Hand Object Re-Orientation. arXiv, arXiv:2111.03043.

[14] Chanrungmaneekul P, Ren K, Grace J, et al., 2023, Non-Parametric Self-Identification and Model Predictive Control of Dexterous In-Hand Manipulation. 2023 IEEE/RSJ International Conference on Intelligent Robots and Systems: 8743–8750.

[15] Weinberg A, Shirizly A, Azulay O, et al., 2024, Survey of Learning-Based Approaches for Robotic In-Hand Manipulation. Frontiers in Robotics and AI, 11: 1455431.

[16] Sintov A, Kimmel A, Wen B, et al., 2020, Tools for Data-Driven Modeling of Within-Hand Manipulation with Underactuated Adaptive Hands. Proceedings of Machine Learning Research, 120: 771–780.

[17] Patidar S, Sieler A, Brock O, 2023, In-Hand Cube Reconfiguration: Simplified. 2023 IEEE/RSJ International Conference on Intelligent Robots and Systems: 8751–8756.

[18] Hess A, Kübler A, Forrai B, et al., 2025, Sampling-Based Model Predictive Control for Dexterous Manipulation on a Biomimetic Tendon-Driven Hand. 2025 IEEE/RSJ International Conference on Intelligent Robots and Systems: 5509–5516.